medRxiv preprint doi: https://doi.org/10.1101/2022.08.20.22278813; this version posted August 22, 2022. The copyright holder for this preprint **(which was not certified by peer review)** is the author/funder, who has granted medRxiv a license to display the preprint in perpetuity.
It is made available under a CC-BY-ND 4.0 International license .

Title

Uncovering personalised glucose responses and circadian rhythms from multiple wearable biosensors with Bayesian dynamical modelling

Authors and affiliations

Nicholas E. Phillips [1,2], Tinh-Hai Collet [2,3]*, Felix Naef [1]*.

[1] Institute of Bioengineering, School of Life Sciences, Ecole Polytechnique Fédérale de Lausanne, Lausanne, Switzerland.
[2] Nutrition Unit, Service of endocrinology, diabetology, nutrition and therapeutic education, Geneva University Hospitals, Geneva, Switzerland.
[3] Diabetes Centre, Faculty of Medicine, University of Geneva, Geneva, Switzerland.

* These authors contributed equally and act both as corresponding authors (tinh-hai.collet@hcuge.ch; felix.naef@epfl.ch).

NOTE: This preprint reports new research that has not been certified by peer review and should not be used to guide clinical practice.

medRxiv preprint doi: https://doi.org/10.1101/2022.08.20.22278813; this version posted August 22, 2022. The copyright holder for this preprint **(which was not certified by peer review)** is the author/funder, who has granted medRxiv a license to display the preprint in perpetuity.
It is made available under a CC-BY-ND 4.0 International license .

Abstract

Wearable biosensors and smartphone applications can measure physiological variables over multiple days in free-living conditions, revealing circadian rhythms and responses to external stressors such as meals and physical activity. Here we develop a probabilistic Bayesian framework to learn interpretable, personal parameters from wearable time series data. We measure food and drink ingestion, glucose dynamics, physical activity, heart rate (HR) and heart rate variability (HRV) in 25 healthy participants over 14 days. Modelling ingestion events with glucose reveals that slow glucose decreases are associated with large postprandial glucose spikes, and we uncover a circadian baseline rhythm in glucose levels with high amplitudes in some individuals. Physical activity and circadian rhythms explain 40-65% of HR variance, whereas the variance explained for HRV is more heterogeneous across individuals (20-80%). Finally, incorporating activity, HR and HRV in the modelled glucose explains an additional 10% glucose variability in some individuals, highlighting the relevance of integrating multiple physiological signals for a complete and predictive understanding of glucose dynamics.

Keywords

Wearable devices, glucose levels, circadian rhythms, mathematical modelling, Bayesian inference

medRxiv preprint doi: https://doi.org/10.1101/2022.08.20.22278813; this version posted August 22, 2022. The copyright holder for this preprint (which was not certified by peer review) is the author/funder, who has granted medRxiv a license to display the preprint in perpetuity.
It is made available under a CC-BY-ND 4.0 International license .

Introduction

Wearable biosensors and smartphone applications can be used by individuals in free-living conditions to measure multiple physiological variables, including glucose levels, food consumption, physical and heart activity. In contrast to traditional lab measurements taken at a single time point, the time series data provided by wearables can reveal the dynamic changes of physiological variables in response to external perturbations and as a function of the time of day. Wearable data has the potential to create a more dynamical systems view of health status[1], but one of the major challenges of personalised medicine will be how to extract the most robust and physiologically meaningful information from these complex time series data.

Glucose regulation is a prime example of a dynamic and complex physiological system, as the body is confronted with irregular inputs (i.e. food intake, especially of carbohydrates) and glucose uptake by organs (e.g. muscles, liver, heart). As such, glycaemic regulation employs a range of homeostatic mechanisms to avoid both low (hypoglycaemic) or high (hyperglycaemic) levels of glucose[2]. After meal consumption, increased insulin secretion by pancreatic beta cells acts to decrease glucose levels by promoting the utilisation of glucose and inhibiting endogenous production, but this glucose-insulin negative feedback loop can become defective in diabetes mellitus through either insulin resistance or beta cell dysfunction[3]. Long-term chronic hyperglycaemia in diabetes mellitus can lead to macrovascular (atherosclerosis and cardiovascular disease) and microvascular (neuropathy, nephropathy, retinopathy) complications[4], and glucose levels show a non-linear and modest association with vascular diseases even in populations without diabetes[5–7].

As glucose homeostasis is inherently dynamic and glucose levels fluctuate throughout the day, continuous glucose monitors (CGMs) have gained popularity as they provide deeper insights into glucose regulation. CGMs measure glucose in interstitial fluid continuously for up to 2 weeks with satisfactory clinical accuracy compared to reference capillary blood glucose values[8], and standardised CGM-derived metrics such as the coefficient of variation (CV, the standard deviation divided by the mean) and the time-in-range (the fraction of time spent within the desired range of 3.9-10.0 mmol/L) have been adopted in clinical practice to assess glycaemic control within diabetic patients[9–11]. At a more fine-grained level, CGMs have been combined with smartphone records of ingestion events to quantify postprandial (post-meal) glycaemic responses (PPGR) in free-living conditions, where the PPGR is often defined as the area under the glucose curve for the two hours following a recorded ingestion event[12–14]. Machine learning predictions of PPGRs using multiple explanatory variables (including blood parameters, dietary habits, anthropometrics, physical activity, and gut microbiota) correlate with the measured PPGRs better than carbohydrate-only predictions[12], showing the potential of wearables to create more personalised nutrition plans.

medRxiv preprint doi: https://doi.org/10.1101/2022.08.20.22278813; this version posted August 22, 2022. The copyright holder for this preprint (which was not certified by peer review) is the author/funder, who has granted medRxiv a license to display the preprint in perpetuity.
It is made available under a CC-BY-ND 4.0 International license .

None-the-less, neither the standardised CGM metrics nor the PPGR approach can explain the complete glucose time series and its fluctuations over the 24-hour clock. Physiological processes in humans follow 24-hour cycles, including blood hormone levels, blood pressure, body temperature, and sleep[15–17]. Energy metabolism is also subject to circadian control via both the endocrine system and direct regulation of metabolites[18–23], and glucose spikes following oral glucose tests are more severe in the evening than the morning[24]. A pre-breakfast rise in glucose levels, termed the “dawn phenomenon”, has been observed since the early 1980s[25,26], but the amplitude and phase of circadian rhythms in baseline glucose levels has thus far not been well described at an individual level. Describing the relative contribution of the circadian clock to the glucose time series would be particularly helpful for the interpretation of the standard 24-hour summary CGM report, which is often used in discussions with patients to identify patterns of low and high glucose values[27].

In addition to CGMs, wearables also allow the measurement of heart activity either optically using photoplethysmography or via electrical signals with electrocardiography. In addition to heart rate (HR), the intervals between each heart beats (interbeat interval) can be used to quantify the heart rate variability (HRV) through a variety of metrics[28], including the root mean square of successive differences (RMSSD) between successive heart beats. HR receives inputs from both the sympathetic nervous system (SNS) and parasympathetic nervous system (PNS), whereas RMSSD is more related to the PNS via vagal nerve activity[29]. The SNS and PNS are sometimes simplistically referred to the “flight or fight" or “rest and digest” branches of the autonomic nervous system and control a diverse range of functions in the body[30]. Plasma glucose levels are negatively associated with HRV[31,32], and a reduction in HRV has been shown to predict the development of autonomic neuropathy before symptom onset amongst diabetic patients[33]. Both HR and HRV are modulated by physical activity, which can now be conveniently measured with a triaxial accelerometer often integrated in wearables. Analogously to meals providing perturbations to the glucose system, physical activity acts as a perturbation to the SNS and PNS systems, and the simultaneous measurement of physical activity, HR and HRV could be used to assess the sensitivity of the autonomic nervous system to physical activity as an external stressor.

In this study, we use multiple wearable sensors to measure glucose levels, HR and HRV in individuals in free-living conditions, in order to quantify for each individual the role of external perturbations (such as ingestion events and physical activity) and baseline circadian rhythms. To achieve this, we build a minimal dynamic model (Supplementary Fig.1) that considers multi-signal interactions, 24-hour rhythms and random fluctuations and infer the parameters for each individual within a Bayesian framework. We first combine the ingestion events recorded with a smartphone app with the glucose time series and show that individuals with a slow response half-life (i.e. a dynamic property) also have the largest postprandial glucose responses. The circadian rhythms in baseline glucose levels are highly personalised in terms of

medRxiv preprint doi: https://doi.org/10.1101/2022.08.20.22278813; this version posted August 22, 2022. The copyright holder for this preprint (which was not certified by peer review) is the author/funder, who has granted medRxiv a license to display the preprint in perpetuity.
It is made available under a CC-BY-ND 4.0 International license .

amplitude and phase. We then analyse physical activity, HR and HRV as a coupled dynamical system and find that the combination of physical activity and circadian baseline rhythms well predict HR for all participants. The physical activity, HR and circadian components explain the vast majority of variance in RMSSD (a proxy for PNS) for some participants, but the ability to exploit the multi-signal coupling was much weaker for others. Finally, the integration of the physical and heart activity explains additional glycaemic variability for some individuals. While our study assessed cross-sectional differences between individuals, future studies will be able to re-use the framework to describe subject-specific longitudinal changes over time in response to interventions and to metabolic diseases.

Results

Measuring multivariable physiological time series in free-living conditions

To quantify the personalised dynamics of individuals in free-living conditions, we measured ingestion events, glucose levels, physical activity, HR and HRV for 25 participants over a two-week period. Participants (16 males, 9 females) were young (mean age 33.0 ± SD 11.0), had normal weight (mean BMI 22.7 ± 2.8 kg/m^2, 1 person with overweight and 1 person with obesity) and a normal blood pressure (systolic 117.6 ± 11.4 mmHg, diastolic 75.3 ± 7.9 mmHg). Participants were asked to record all food and drink consumption and add a manual free text annotation of the content with the smartphone application MyCircadianClock[34]. Each ingestion event was automatically timestamped by the app. The adherence (defined as at least 2 meals separated by at least 5 hours in a given day[35]) was above 83% for all participants (Supplementary Table 1). Participants were also asked to log physical exercise using the app.

We measured glucose levels continuously using the Abbott FreeStyle Libre Pro CGM device, which records interstitial glucose levels every 15 minutes over a two-week period. As the device is blinded, participants were unable to access their glucose data during the study period thus avoiding feedback on their eating behaviour. Five participants wore two sensors (on different arms), with the aim of validating that parameters estimated from the model were consistent between the two sensors (noted ID .A and .B in the figures below). We often saw long-term trends within the time series glucose data, which could be related to sensor drift or a slow-changing biological variable of unknown origin. To pre-process the glucose data, we removed such long-term trends with a non-parametric regression model with a time-scale of two days (see Methods). Physical activity, HR and HRV were measured for each participant over the two-week study period using the CamNTech ActiHeart device, and the physical and heart activity data was also blinded to participants during the study.

medRxiv preprint doi: https://doi.org/10.1101/2022.08.20.22278813; this version posted August 22, 2022. The copyright holder for this preprint (which was not certified by peer review) is the author/funder, who has granted medRxiv a license to display the preprint in perpetuity.
It is made available under a CC-BY-ND 4.0 International license .

Multi-wearable time series data reveal complex dynamical responses as a function of external inputs and time of day

As an exploratory data visualisation, we superposed the recorded days of glucose data based on time of day and found strong inter-individual heterogeneity in the mean 24-hour pattern, with the highest mean glucose level occurring in the morning, afternoon or evening depending on the individual (Fig.1a, all participants shown in Supplementary Fig.2). These unique 24-hour trends could be caused by either food or drink ingestion (i.e. external perturbations) and/or an underlying circadian baseline rhythm, and this motivated the inclusion of both ingestion events and circadian rhythms in the model of glucose dynamics as separate components with learnable parameters.

Further exploratory analysis of the multiple wearable signals showed rich interactions between the five measured variables (i.e. meals, glucose, activity, HR and HRV). As expected, glucose levels often rose following ingestion events, and for some of the individuals, recorded meals seemed to lead to large, predictable peaks in glucose (Fig.1b, ID 14 and 23), while for others this relationship appeared to be more complex, with small postprandial glucose spikes that were barely larger than the glucose fluctuations between meals (Fig.1b, ID 06). Compared to CGM analysis methods that focus exclusively on PPGRs, our goal was to dynamically model the entire glucose time series over 2 weeks, including the fluctuating glucose levels during periods between ingestion events.

Visual inspection of the physical and heart activity data showed that spikes in physical activity typically coincided with an increased HR and HRV (as measured with $RMSSD^{-1}$) (Fig.1c-d). By creating a joint dynamical model of the three signals (physical activity, HR and HRV), we aimed to uncover the inter-individual heterogeneity in response dynamics, the underlying rhythms, as well as the coupling between the multiple signals.

Finally, we observed spikes in glucose levels following physical activity for some individuals (Fig.1b, ID 23), which could be caused by the release of glucose from the liver via glucagon or the effect of adrenaline. However, to establish more firmly whether physical and heart activity signals help explain glucose variation, we developed a dynamical model to formally assess to which extent the total glucose signal across the two-week study period is predictable by the combined meal, physical, HR and HRV data (Supplementary Fig.1).

medRxiv preprint doi: https://doi.org/10.1101/2022.08.20.22278813; this version posted August 22, 2022. The copyright holder for this preprint **(which was not certified by peer review)** is the author/funder, who has granted medRxiv a license to display the preprint in perpetuity.
It is made available under a CC-BY-ND 4.0 International license .

Slow glucose dynamics is associated with large postprandial glucose spikes

We will first construct a mathematical model of glucose dynamics that incorporates food and drink ingestion timestamped events, circadian rhythms in baseline glucose levels and random fluctuations in glucose levels (we will later add the physical and heart activity variables). Following from the visual data exploration (Fig.1) and physiological knowledge, we built a minimal dynamical model that included the following four features: i) the ability to produce a continuous postprandial glucose response following an ingestion event, ii) negative feedback (due to the regulating action of insulin, Supplementary Fig.1), iii) a random component that captures the glucose fluctuations between meals, iv) a circadian baseline rhythm (discussed in next section).

We model the glucose dynamics using a negative feedback model (see Methods), where ingestion events act to perturb glucose to higher levels. After the ingestion causes an increase, the glucose levels return to their steady-state values (i.e. reflecting homeostasis), but the decay kinetics and precise shape of the response will depend on the individual parameters of the model. The glucose dynamics is also subjected to random perturbations to account for fluctuations in the data, meaning that the glucose time series data can show noisy deviations from the idealised, deterministic meal response.

The glucose dynamics model can then be summarised with three parameters controlling the individual-specific response to a meal perturbation (or random fluctuation), namely a half-life reflecting the time taken for glucose to return to baseline levels, the mean increase in glucose levels caused by meal consumption (referred to as the average meal height) and a damping coefficient specifying whether the response profile is akin to an overdamped (a rapid glucose increases followed by a monotonous slower decay i.e. non-dipping) or an underdamped (leading to a slower initial increase followed by decay and overshoot, i.e. dipping) response. For each participant, the entire glucose time-series is probabilistically matched to the model using a Gaussian state space model (a.k.a. a Kalman filter) and we infer each of the model parameters using Markov Chain Monte Carlo (MCMC) sampling within a Bayesian framework that yields uncertainty estimates for each parameter (Methods and Supplementary Information). We first verified model performance by assessing the correlation coefficient between the fitted meal response function and the data (Fig. 2a). The correlation coefficient generally ranged from 0.5-0.8 but was particularly low for participant ID 04. Visual inspection of this participant's raw data showed large glucose spikes following physical activity, which we address at a later stage of the modelling. While all model parameters are shown in Supplementary Fig.3, here we focus on the three summary metrics of the glucose dynamics.

medRxiv preprint doi: https://doi.org/10.1101/2022.08.20.22278813; this version posted August 22, 2022. The copyright holder for this preprint **(which was not certified by peer review)** is the author/funder, who has granted medRxiv a license to display the preprint in perpetuity.
It is made available under a CC-BY-ND 4.0 International license .

Response half-lives ranged from 1h to 2.2h (Fig.2b) and average meal response heights ranged from 0.5 mmol/L to 1.5 mmol/L (Fig.2c). Across participants we found a positive relationship between response half-lives and average meal heights, with slower glucose response half-lives associated with larger postprandial glucose spikes (Fig.2d). This suggested that postprandial glucose control (i.e. the size of glucose spikes following meals) depends on glucose clearance time, which might be determined physiologically by insulin sensitivity or beta cell function (Discussion).

The damping coefficients describing the shapes of glucose responses were clustered around 0 across all participants (Fig.2e), where values of 0 represent "critical" damping at the border between overdamped (non-dipping profiles, damping coefficient >0) and underdamped (profiles with a dip, damping coefficient <0). Interestingly, glucose responses were proposed to be critically damped in an early glucose model[36], which would be consistent with our finding that the inferred values are scattered around zero. However, subject-to-subject variability is clearly found, with participant ID 14 showing a clear underdamped glucose response compared to the critically damped response in ID 23 (Fig.2f-h). While the fitted model that uses meal responses and circadian time (orange) is a smooth function that shows deviations from the glucose data (blue, Fig.2g-h), the full model that also adds random fluctuations produces glucose traces that closely resemble the glucose data (Supplementary Fig. 4).

We used linear regression to quantify the relationships between the glucose model parameters and the glucose coefficient of variation (CV) derived from the glucose data, which is a metric of glycaemic control used in the clinical settings[9,11]. We found statistically significant relationships with both the response half-lives ($p=0.03$) and average meal heights ($p=0.01$) (R^2 using both variables = 0.63). On the other hand, the damping coefficient was not significantly associated with glucose CV, but the shape of the glucose response might otherwise play a role in other aspects of glucose dynamics such as overshooting and hunger[37]. Our results highlight that the glucose response half-life is playing a significant role in glycaemic control and may be an interesting parameter to estimate for both fundamental research and clinical purposes.

Circadian rhythms in baseline glucose levels show large inter-individual variability

In addition to the input from ingestion events, the glucose model also allows for an underlying circadian rhythm in glucose levels described with three parameters: a baseline level that specifies the glucose at the trough of the oscillation, an amplitude parameter denoting the difference between the trough and peak of the oscillation, and a parameter that sets the peak time of the oscillation.

medRxiv preprint doi: https://doi.org/10.1101/2022.08.20.22278813; this version posted August 22, 2022. The copyright holder for this preprint (which was not certified by peer review) is the author/funder, who has granted medRxiv a license to display the preprint in perpetuity.
It is made available under a CC-BY-ND 4.0 International license .

The amplitudes of underlying circadian glucose rhythms were highly variable between participants (Fig. 3a), being virtually null for some participants while exceeding 1 mmol/L for others (Fig. 3b, ID 03 and 07, respectively). The association between the circadian baseline amplitude and glucose CV was not statistically significant, possibly due to the fact that the contribution of meals dominates in terms of explained glycaemic variability (Fig. 3e), and individuals with the largest amplitude circadian oscillations could still maintain low glucose CV.

The confidence intervals for the peak times of the circadian oscillations showed large differences between participants, with tight confidence intervals for participants with large amplitudes and wide intervals for participants with weaker amplitudes (Fig. 3c). This relationship is probably caused by a low signal-to-noise ratio and suggests that the circadian peak time cannot be reliably inferred for participants with a low circadian amplitude. While the peak times of the circadian underlying trend typically fell in the mid-afternoon, there were several notable exceptions. For example, participant ID 20 had a phase at 10:00 while it occurred much later for participant ID 17, falling at 20:00 (Fig. 3d).

Overall, the underlying circadian glucose rhythm plays an important role in glucose dynamics and could explain >15% of glycaemic variability in addition to the meal model for participants with large amplitudes (Fig. 3e). Given that the study was observational, we do not know whether it would be possible to modify either the peak time or amplitude of this rhythm, but these personalised parameters should prove to be useful in applications such as personalised meal timing (Discussion).

The multi-signal coupling between physical and heart activity varies between individuals

For the physical and heart activity data, we first considered the impact of physical activity and underlying circadian rhythms on heart rate (HR, Supplementary Fig.1, all inferred model parameters shown in Supplementary Fig. 5). In a similar manner to ingestion events acting as external inputs into glucose levels, we modelled physical activity as a positive input into HR (i.e. activity acts to increase HR).

The combination of circadian rhythms and of physical activity input was consistently predictive for HR, explaining 40-65% of HR variance across all participants (Fig.4a). Fig. 4b-c shows an example of the predicted HR (orange) for two different participants using both the underlying circadian rhythm (black) and integrating the physical activity (green). While the circadian contribution to the explained HR variance differs for these two participants (Fig.4 a), the correlation between the predicted and observed HR was around 0.8 for both participants, demonstrating that time of day and activity state are necessary for optimal personalised modelling of HR.

medRxiv preprint doi: https://doi.org/10.1101/2022.08.20.22278813; this version posted August 22, 2022. The copyright holder for this preprint (which was not certified by peer review) is the author/funder, who has granted medRxiv a license to display the preprint in perpetuity.
It is made available under a CC-BY-ND 4.0 International license .

The ability to predict HRV was, in contrast, much more heterogeneous between participants. HR and HRV (assessed with $RMSSD^{-1}$) share common physiological inputs, where HR is controlled by the PNS and SNS while RMSSD is predominantly influenced by the PNS[28]. The shared inputs may cause correlations between the HR and HRV time series, which we modelled by including a correlation parameter between HR and HRV fluctuations (Methods). In addition to inputs from physical activity and the underlying circadian rhythm, we evaluated whether the correlations between HR and HRV could be exploited by using HR to predict HRV (which is technically more difficult to measure than HR).

The ability to predict HRV varied significantly across individuals with (total variance explained between 20-80%, Fig. 4d). This notable difference in predictability is illustrated in Fig. 4d, showing a favourable prediction for participant ID 25 (R = 0.89) compared to ID 14 (R = 0.44). For ID 25, the HR signal explained 40% of the variance compared to using just activity and circadian rhythm, but for ID 14 the addition of HR makes no difference to HRV prediction (Fig. 4e-f). Given that RMSSD is considered a proxy for PNS (via the vagus nerve) activity, the strong relationship between HR and RMSSD for ID 25 suggests that HR is more tightly coupled to PNS activity than for ID 14. Of note, ID 14 was previously diagnosed with diabetes but was currently treated only with lifestyle measures (and not pharmacological treatment) and ANS dysfunction is a known complication of diabetes [38].

Integrating physical and heart activity signals helps explain glycaemic dynamics for some individuals

As a final modelling step, we integrated the physical and heart activity signals with the glucose-meals model to quantify how much of the glucose dynamics can be accounted for with physical activity, HR and HRV (Supplementary Fig.1). To simplify the model inference problem, the parameters describing the physical and heart activity model in isolation were locked to their posterior mean values, and we added three new parameters that describe the input of physical activity, HR and HRV on glucose levels, respectively (Supplementary Fig.1). These influences were left unconstrained and could have a positive, negative or zero effect on glucose levels.

Fitting the parameters to the data revealed that the effect of physical activity on glucose (parameter $C_{5,1}$) was generally negative, the effect of HR (parameter $C_{5,2}$) was generally positive and the effect of HRV (parameter $C_{5,3}$) was typically neutral across all participants (Fig.5 a-c). Given that the raw data showed glucose spikes during some periods of exercise (Fig.1 d), the negative influence of physical activity on glucose ($C_{5,1}$) was not fully expected. To test the robustness of this prediction, we therefore refitted the data using three simpler models, where there was only one input at a time from the physical and heart activity signals (Supplementary Fig.6). The influence of physical activity on glucose remained negative even when it was the sole Actiheart input into glucose levels, further suggesting that the overall effect of

medRxiv preprint doi: https://doi.org/10.1101/2022.08.20.22278813; this version posted August 22, 2022. The copyright holder for this preprint (which was not certified by peer review) is the author/funder, who has granted medRxiv a license to display the preprint in perpetuity.
It is made available under a CC-BY-ND 4.0 International license .

physical activity is to deplete glucose levels. Meanwhile, as HR acts to increase glucose levels ($C_{5,2}$), increased HR during intense exercise can still lead to a net increase in predicted glucose levels. Overall, the total amount of additional explained variance contributed by the Actiheart signals was modest for most participants but contributed up to 15% in certain individuals (Fig. 5b).

Amongst the participants whose glucose dynamics benefit most from the physical and heart activity signals, the mode of action also differed. For participant ID 04, the inclusion of the physical and heart activity signals allowed for at least partial prediction of exercise-induced glucose spikes that were otherwise absent from the glucose model that contained meals only (Fig. 5c). For participant ID 08, which also showed a benefit of including physical and heart activity data, there were no notable isolated glucose spikes that were predicted by the physical and heart activity data. Instead, the linear combination of the physical and heart activity variables (weighted according to the inferred coefficients $C_{5,1}$-$C_{5,3}$) appeared to track the glucose levels (Fig. 5d), and the cross-correlation profile showed a maximum correlation between the two signals with no time delay (Fig. 5e). This suggests that for this type of action, the physical and heart activity signals make a more diffuse contribution to the prediction of glucose levels that is more related to baseline trends spread over the time series.

Discussion

A new generation of wearable biosensors can measure multiple physiological variables with high temporal resolution over multiple days. Here we developed a stochastic dynamical model combined with Bayesian learning to capture the full time series for each participant and provide interpretable personalised parameters that reflect responses to external perturbations and circadian rhythms.

Combining the ingestion events timestamped by the smartphone app with the glucose time series, we found that slow glucose dynamics are associated with large postprandial glucose spikes. Mechanistically, slow glucose disposal could relate with the quantity of ingested carbohydrates, the rate of gut absorption[39], its metabolism[40], suppression of endogenous glucose production[41], insulin resistance or beta cell function[3]. Moreover, we also detected highly personalised circadian rhythms in the underlying glucose levels. While diurnal rhythms in beta cell function and insulin sensitivity have been shown at an average level within healthy populations[42], it was unexpected to see such large differences in circadian glucose amplitude and phase between individuals. Future studies will determine whether this circadian glucose trendline is predictive of responses to specific meal times, e.g. in time-restricted eating, an intervention which restricts eating to a specific window within the 24-hour clock[43].

medRxiv preprint doi: https://doi.org/10.1101/2022.08.20.22278813; this version posted August 22, 2022. The copyright holder for this preprint (which was not certified by peer review) is the author/funder, who has granted medRxiv a license to display the preprint in perpetuity.
It is made available under a CC-BY-ND 4.0 International license .

Many different models of glucose dynamics have been proposed over the last several decades[44–46], ranging from minimal models[47] to more detailed simulators with dozens of parameters[48]. There are many possible extensions that could be added to the glucose model. For simplicity and to ease identifiability, we assumed that the shape of each meal response was conserved within each individual (but variable across individuals) while the height was learnt for each unique ingestion event. Given that the rate of meal absorption likely depends on meal constituents such as fat, fibre and protein content[14], the response shape of each meal could indeed vary, although the addition of meal-specific response shapes would effectively double the number of meal-related parameters. Our two-dimensional linear model is admittedly a coarse-grained approximation of the full glucose metabolism system, although linear models with more variables (representing glucose and insulin in different compartments) have been deployed in artificial pancreas devices and are at the forefront of computer-assisted glucose management in diabetes[49,50]. More complex nonlinear dependencies and long-range memory could be captured for example with flexible neural networks[51–54]. In contrast to the artificial pancreas, where highly accurate short-range forecasting is desirable, our main goal was to extract model-based summary metrics for distilled and multi-metric diagnostics.

Recent efforts have attempted to utilise additional multimodal wearable signals to either improve glucose forecasting or provide more accessible proxies for glucose without using CGMs [55–57]. The physical and heart activity data explained up to 15% of glucose variability in our study. From a clinical perspective, the incorporation of these additional signals might help both patients and clinicians understand glucose dynamics that seem otherwise disconnected from meal consumption (e.g. Fig. 5e). A potential limitation of our approach is again the use of a relatively simple linear model, which may not be able to capture more complex phenomena such as eventual decreases in hepatic glucose production during prolonged exercise[58]. However, a recent study based on deep learning found the addition of wristband activity data improved the root mean square error of 60-minute glucose forecasting by 2.25 mg/dL from a baseline of 35.3 mg/dL, and hence more substantial improvements in glucose predictions may prove to be a difficult challenge even with more flexible models[59].

Within healthcare, there is increasing interest in the use of digital twins[60,61] that integrate multiple types of clinical data to devise personalised treatments and perform risk modelling. As our approach contains interpretable parameters, it would also be possible to explore hypothetical situations by altering parameters (such as circadian amplitude or glucose response time) and simulating from the model. Our data is from a single two-week period, but with multiple measurement periods it would be possible to perform significance testing to detect longitudinal parameter changes over time and across clinical interventions. On a practical level, one of the main advantages of health measurement with wearable biosensors is the relative rapidity of the experimental pipeline: in our study it took a team of two researchers

medRxiv preprint doi: https://doi.org/10.1101/2022.08.20.22278813; this version posted August 22, 2022. The copyright holder for this preprint (which was not certified by peer review) is the author/funder, who has granted medRxiv a license to display the preprint in perpetuity.
It is made available under a CC-BY-ND 4.0 International license .

two days to complete questionnaires and set up devices for all 25 participants simultaneously. Overall, capturing circadian rhythms and interactions between different physiological subsystems with a multi-wearable approach offers a dynamic and personalised description of cardiometabolic health states.

Methods

Devices and experimental design

The Multi-Sensor Study (MSS) was approved by the local ethics committee (CER-VD, BASEC no. 2019-02245) and each participant signed a written informed consent. Recruitment was performed via posters at the École polytechnique fédérale de Lausanne (EPFL), Lausanne University Hospital (CHUV) and the University of Lausanne (UNIL) and via presentations given in the EPFL School of Life Sciences. As part of our recruitment strategy we actively attempted to recruit motivated participants that felt highly confident of recording all of their data for two weeks.

We included adults aged ≥ 18 years, with a smartphone compatible with the MyCircadianClock app (iOS or Android systems[34]) and able to take pictures of food/drinks, and who self-identified as disciplined enough and motivated to record all data for two weeks. The exclusion criteria were major illness/fever, surgery over the previous month, eating disorder, major mental illness, unable to give informed consent, taking medicines including paracetamol, aspirin or vitamin C supplements, enrolled in another interventional clinical trial (medication, medical device), shift work or travel to a different time zone before and during the study.

At baseline, we collected data on demographics, medical history, physical activity (short form of International Physical Activity Questionnaire, IPAQ-SF[62], chronotype (The Munich ChronoType Questionnaire[63], sleeping habits (Pittsburgh Sleep Quality Index[64] and eating timing (with a custom questionnaire on eating habits during work and free days).

For each participant, we collected data for two weeks using the following devices: 1) Timestamps of food/drinks and text annotations collected with the smartphone application (app) MyCircadianClock[34]; 2) Continuous glucose monitoring (CGM) using the FreeStyle Libre Pro device (Abbott); 3) Physical activity, heart rate (HR) and heart rate variability (HRV using $RMSSD^{-1}$) using the *ActiHeart* device (CamNTech). While the Actiheart device is waterproof, participants were permitted to briefly remove the device during showers and baths. Information on device technical failure and handling of missing data and data quality is included in the Supplementary Information.

medRxiv preprint doi: https://doi.org/10.1101/2022.08.20.22278813; this version posted August 22, 2022. The copyright holder for this preprint **(which was not certified by peer review)** is the author/funder, who has granted medRxiv a license to display the preprint in perpetuity.
It is made available under a CC-BY-ND 4.0 International license .

Pre-processing CGM data

We used nonparametric regression with Gaussian processes (GPs) to remove the long-term trends observed in the data. After mean-centring the data, we fitted a GP with a squared exponential kernel $K_{\mathrm{SE}}(t,t') = \alpha \exp\left(-\frac{|t-t'|^2}{2l^2}\right)$ and a length scale *l*=48 hours using GPflow.

Data analysis

See the Supplementary Information for detailed computational methods which are summarised here. We use a linear Gaussian state space model (otherwise known as a Kalman filter) to analyse the time series generated by the wearable devices, which was implemented using the 'LinearGaussianStateSpaceModel' distribution within TensorFlow Probability[65]. We will first describe the general data analysis framework before providing details on each of the three models used. For each model we define a dynamic model that describes the time evolution of the underlying physiological variables and a measurement model that incorporates measurement noise. For the dynamic model, we use a system of stochastic differential equations (SDEs)

$$\mathrm{dx(t)} = \mathrm{Wx(t)dt} + \mathrm{d\beta},$$

where W is a matrix describing the interactions between the variables and β is a brownian noise term with covariance matrix Q. The specific forms of W and Q are unique for each model and will be described below. To keep the model exact while benefiting from the generic framework of Gaussian state space models (a.k.a. as Kalman filters), we then convert this system of continuous-time SDEs into a model where time is discrete (see Supplementary Information for details).

$$\mathrm{x(t_k)} = \mathrm{F_{k-1}x(t_{k-1})} + \mathrm{N(0,\Sigma_{k-1})},$$

where $\mathrm{F_k}$ is the state-transition model and Q is the covariance of the process noise. The measurement model describes the observation process and assumes that variables are observed with normally distributed measurement noise

$$\mathrm{y(t_k)} = \mathrm{H_k x(t_k)} + \mathrm{N(m_k, R_k)},$$

where H_k is the observation matrix and m_k and R_k represents the mean and covariance of the observation noise, respectively. The goal is to use the wearable time series data $y_{1:T}$ to estimate parameters (denoted by θ) for each participant. Within a Bayesian inference framework, the parameters of the model can be estimated from the data as follows

$$\mathrm{p(\theta \mid y_{1:T})} \propto \mathrm{p(\theta) p(y_k \mid \theta)},$$

medRxiv preprint doi: https://doi.org/10.1101/2022.08.20.22278813; this version posted August 22, 2022. The copyright holder for this preprint (which was not certified by peer review) is the author/funder, who has granted medRxiv a license to display the preprint in perpetuity.
It is made available under a CC-BY-ND 4.0 International license .

where $p(\theta)$ is the prior distribution of parameters and $p(y_{1:T} \mid \theta)$ is the likelihood of observing the temporal data $y_{1:T}$ given the set of parameters θ. Considering the time series sequence of data, the likelihood term for a given set of parameters θ can be expressed as

$$p(y_{1:T} \mid \theta) = p(y_1 \mid \theta) \prod_{k=2}^{T} p(y_k \mid y_{1:k-1}, \theta),$$

and the sequence of distributions $p(y_k \mid y_{1:k-1}, \theta)$ are calculated within a Kalman filtering framework. Once the likelihood and priors are specified for each model, we used the Hamiltonian Monte Carlo sampler provided within TensorFlow Probability to sample model parameters from the posterior distribution using 4 different chains with 10,000 samples each. See Supplementary Information for further details on MCMC scheme.

Model 1: glucose model

We model glucose dynamics (Supplementary Fig.1) with a two-dimensional system of SDEs, where the second variable x_{GLUC2} represents the glucose levels and the first variable x_{GLUC1} represents an unobserved latent variable that allows negative feedback within the system. In matrix form, the model is expressed as follows

$$d\mathbf{x}(t) = W\mathbf{x}(t)dt + d\boldsymbol{\beta}$$

$$\mathbf{x}(t) = \begin{bmatrix} x_{GLUC1}(t) \\ x_{GLUC2}(t) \end{bmatrix}, W = \begin{bmatrix} -A_{11} & -A_{12} \\ A_{21} & -A_{22} \end{bmatrix}, Q = \begin{bmatrix} 0 & 0 \\ 0 & B_{22} \end{bmatrix},$$

and where the coefficients A_{ij} are constrained to be positive. The covariance of the brownian noise term β is given by Q.

We incorporate meal events (that are recorded at time t_m) as producing a response function $r_m(t)$ (see Supplementary Information for precise functional form), and then the total meal function is the sum over all individual meal responses

$$r(t) = \sum_{M} r_m(t)$$

We also add an underlying circadian rhythm in glucose levels using a sinusoidal function

$$g(t) = A_{0,GLUC} + A_{1,GLUC}(1 + \cos(\omega t - \phi_{GLUC}))/2$$

where $A_{0,GLUC}$ is the baseline level, $A_{1,GLUC}$ is the amplitude, ω is the frequency (fixed at $2\pi/24$), and ϕ_{GLUC} is the peak time of the maximum. The observation model for the glucose model is then as follows

medRxiv preprint doi: https://doi.org/10.1101/2022.08.20.22278813; this version posted August 22, 2022. The copyright holder for this preprint (which was not certified by peer review) is the author/funder, who has granted medRxiv a license to display the preprint in perpetuity.
It is made available under a CC-BY-ND 4.0 International license .

$$\mathbf{y}(t_k) = H_k\mathbf{x}(t_k) + N(\mathbf{m}_k, R_k)$$
$$H_k = [0,1]\,, \mathbf{m}_k = r(t) + g(t), R_k \quad = \sigma_{glu}^2$$

Model 2 : physical and heart activity model

We model glucose dynamics (Supplementary Fig.1) with a with a three-dimensional system of SDEs, where the first variable x_{ACT} represents physical activity, the second variable x_{HR} represents heart rate and the third variable x_{HRV} represents heart rate variability, where we use the inverse of the root mean square of successive differences between normal heartbeats (RMSSD^{-1}). We normalise all three variables by their respective standard deviations before inferring parameters. In matrix form, the model is expressed as follows

$$\mathrm{d}\mathbf{x}(t) = W\mathbf{x}(t)\mathrm{d}t + \mathrm{d}\boldsymbol{\beta},$$
$$\mathbf{x}(t) = \begin{bmatrix} x_{\mathrm{ACT}}(t) \\ x_{\mathrm{HR}}(t) \\ x_{\mathrm{HRV}}(t) \end{bmatrix} W = \begin{bmatrix} -C_{11} & 0 & 0 \\ C_{21} & -C_{22} & 0 \\ C_{31} & 0 & -C_{33} \end{bmatrix} Q = \begin{pmatrix} D_{11} & 0 & 0 \\ 0 & D_{22} & \rho\sqrt{D_{22}D_{33}} \\ 0 & \rho\sqrt{D_{22}D_{33}} & D_{33} \end{pmatrix},$$

and where the coefficients C_{ij} are constrained to be positive and the covariance of the brownian noise term β is given by Q. The observation model is then given by

$$\mathbf{y}(t_k) = H_k\mathbf{x}(t_k) + N(\mathbf{m}_k, R_k),$$
$$\mathbf{m}_k = \begin{bmatrix} g_{\mathrm{ACT}}(t) \\ g_{\mathrm{HR}}(t) \\ g_{\mathrm{HRV}}(t) \end{bmatrix}, H_k = \begin{pmatrix} 1 & 0 & 0 \\ 0 & 1 & 0 \\ 0 & 0 & 1 \end{pmatrix}, R_k = \begin{bmatrix} \sigma_{\mathrm{ACT}}^2 & 0 & 0 \\ 0 & \sigma_{\mathrm{HR}}^2 & 0 \\ 0 & 0 & \sigma_{\mathrm{HRV}}^2 \end{bmatrix}$$

where $g_{\mathrm{ACT}}(t)$, $g_{\mathrm{HR}}(t)$ and $g_{\mathrm{HRV}}(t)$ are circadian oscillatory functions (Supplementary Information).

Model 3: combined model

The final model (Supplementary Fig.1) connects the Actiheart signals with glucose dynamics by stitching the previous glucose and Actiheart models together. The glucose and Actiheart models are otherwise left unchanged, but there is an introduction of three new parameters C_{51}, C_{52} and C_{53} that describe the effect of physical activity, HR and HRV on glucose levels. These three parameters are left unconstrained and can take either positive or negative values.

medRxiv preprint doi: https://doi.org/10.1101/2022.08.20.22278813; this version posted August 22, 2022. The copyright holder for this preprint (which was not certified by peer review) is the author/funder, who has granted medRxiv a license to display the preprint in perpetuity.
It is made available under a CC-BY-ND 4.0 International license .

$$\mathrm{d}\mathbf{x}(t) = W\mathbf{x}(t)\mathrm{d}t + \mathrm{d}\boldsymbol{\beta}$$

$$\mathbf{x}(t) = \begin{bmatrix} x_{\mathrm{ACT}}(t) \\ x_{\mathrm{HR}}(t) \\ x_{\mathrm{HRV}}(t) \\ x_{\mathrm{GLUC1}}(t) \\ x_{\mathrm{GLUC2}}(t) \end{bmatrix} W = \begin{bmatrix} -C_{11} & 0 & 0 & 0 & 0 \\ C_{21} & -C_{22} & 0 & 0 & 0 \\ C_{31} & 0 & -C_{33} & 0 & 0 \\ 0 & 0 & 0 & -A_{11} & -A_{12} \\ C_{51} & C_{52} & C_{53} & A_{21} & -A_{22} \end{bmatrix} Q = \begin{bmatrix} D_{11} & 0 & 0 & 0 & 0 \\ 0 & D_{22} & \rho\sqrt{D_{22}D_{33}} & 0 & 0 \\ 0 & \rho\sqrt{D_{22}D_{33}} & D_{33} & 0 & 0 \\ 0 & 0 & 0 & 0 & 0 \\ 0 & 0 & 0 & 0 & B_{22} \end{bmatrix}$$

The observation model is then given by

$$\mathbf{y}_k = H_k\mathbf{x}(t_k) + N(\mathbf{m}_k, R_k)$$

$$\mathbf{m}_k = \begin{bmatrix} g_{\mathrm{ACT}}(t) \\ g_{\mathrm{HR}}(t) \\ g_{\mathrm{HRV}}(t) \\ g_{\mathrm{GLUC}}(t) \end{bmatrix}, H_k = \begin{pmatrix} 1 & 0 & 0 & 0 & 0 \\ 0 & 1 & 0 & 0 & 0 \\ 0 & 0 & 1 & 0 & 0 \\ 0 & 0 & 0 & 0 & 1 \end{pmatrix}, R_k = \begin{bmatrix} \sigma^2_{\mathrm{ACT}} & 0 & 0 & 0 \\ 0 & \sigma^2_{\mathrm{HR}} & 0 & 0 \\ 0 & 0 & \sigma^2_{\mathrm{HRV}} & 0 \\ 0 & 0 & 0 & \sigma^2_{\mathrm{gluc}} \end{bmatrix}$$

Acknowledgments

The authors wish to thank all participants in the study and the team of Professor Satchidananda Panda (Salk Institute) for the use of the *myCircadianClock* smartphone application. This project was supported by the grant #2018-427 of the Strategic Focal Area “Personalized Health and Related Technologies (PHRT)” of the ETH Domain to N.P. Dr. T-H Collet’s research is supported by grants from the Swiss National Science Foundation (PZ00P3-167826), the Leenaards Foundation (Translational Medicine 2019 call), the Vontobel Foundation, the Swiss Society of Endocrinology and Diabetes, and the Swiss Multiple Sclerosis Society. The work in the Naef lab and purchase of the wearable devices was supported by the EPFL.

Author contributions

Conceptualization: N.E.P., T.-H.C., F.N.; Methodology, N.E.P., T.-H.C., F.N.; Data collection: N.E.P., T.-H.C.; Computation and data analysis: N.E.P.; Data visualisation, N.E.P., T.H.C., F.N.; Writing: original draft preparation, N.E.P.; Writing: review and editing, N.E.P., T.-H.C., F.N.; Project administration: N.E.P., T.-H.C., F.N.; Supervision: T.-H.C., F.N.; Funding acquisition: N.E.P., T.-H.C., F.N. All authors have read and agreed to the published version of the manuscript.

Competing interests

The authors declare no competing interests.

Data availability

The data will be made available after publication in an anonymised form.

medRxiv preprint doi: https://doi.org/10.1101/2022.08.20.22278813; this version posted August 22, 2022. The copyright holder for this preprint **(which was not certified by peer review)** is the author/funder, who has granted medRxiv a license to display the preprint in perpetuity.
It is made available under a CC-BY-ND 4.0 International license .

Code availability

The code will be made available on github after publication.

Figure legends

Fig.1. Exploratory analysis of wearable signals: examples of 24-hour trends and responses to external stressors. (a) Continuous glucose monitoring (CGM) data: superposition of all recorded days of data shown on the same 24-hour scale for three different participants (see related Supplementary Fig.2 for all participants). Black: average over all days; coloured lines: data for individual days; time axis: wall clock time. (b) Selected day examples of CGM glucose levels alongside recorded ingestion events for three participants (same individuals shown in panels B-D). Blue: glucose levels; green shade: recorded activity events; time axis: wall clock time; vertical dotted lines: ingestion events. (c) Selected day examples of physical activity measured with the *Actiheart* device. Green: physical activity; green shade: recorded activity events; time axis, clock time. (d) Selected day examples of HR and HRV measured with the *Actiheart* device. Green shade: recorded activity events; purple: heart rate variability (HRV) (quantified with $RMSSD^{-1}$ in ms^{-1}); red: heart rate (HR) in beats per min. (bpm); time axis: wall clock time.

Fig. 2. Characterising participant-specific post-meal glycaemic responses. (a) Posterior distributions (shown as boxplots) of the correlation between the inferred model (including meals and circadian time) and the glucose CGM data for each participant. The boxplots represent the 25th, median (50th) and 75th percentiles of the posterior distribution and the whiskers represent the 5th and 95th percentiles. (b) The inferred glucose response half-life for each participant, defined as the model-predicted time it would take for glucose levels to fall to 0.5 mmol/L following a peak of 1 mmol/L. (c) The average meal glucose spike height calculated as the mean height over all meals consumed during the experiment. (d) The average meal height as a function of the glucose meal response half-life. Points represent the mean posterior values for each participant. (e) Damping coefficients (see Methods). (f) Average meal response profiles using the posterior mean parameter values. (g-h) Examples comparing the CGM data (blue) with the model prediction incorporating circadian dynamics (black) plus meal consumption (orange) for two participants with overdamped and underdamped dynamics, respectively. The timestamps of meals are shown as black dashed lines. Participant order is the same in Fig.2 and 3.

Fig.3. Amplitudes and peak times of circadian baseline levels of glucose are highly heterogeneous between participants. (a) The amplitude of the 24-hour sinusoidal circadian rhythm in glucose levels after model fitting to the CGM data for all participants. The boxes represent the 25th, median (50th) and 75th percentiles of the posterior distribution and the whiskers represent the 5th and 95th percentiles. (b)

medRxiv preprint doi: https://doi.org/10.1101/2022.08.20.22278813; this version posted August 22, 2022. The copyright holder for this preprint **(which was not certified by peer review)** is the author/funder, who has granted medRxiv a license to display the preprint in perpetuity.
It is made available under a CC-BY-ND 4.0 International license .

Example of participants with a high (ID 07) and low (ID 03) amplitude glucose circadian rhythm. Blue, CGM data; black, fitted model of circadian baseline (using mean posterior parameter values). (c) The circadian phase of the glucose circadian rhythm across all participants. (d) Examples showing two participants with large phase difference in underlying glucose rhythm (ID 20 peak phase: 10:00, ID 17 peak phase: 20:00). (e) The explained variance in glucose levels using just the meal component of the model (light orange) compared with the inclusion of the circadian rhythm (dark orange). Participant order is the same in Fig.2 and 3.

Fig. 4. HRV predictions using multi-signal inputs and circadian rhythms are more heterogeneous than for HR. (a) the amount of variance of the HR signal explained by circadian rhythms (light orange) and a combined model with circadian rhythms and physical activity (dark orange). (b,c) Examples comparing HR data with model predictions for two participants. Red: HR data; black: baseline circadian rhythm; green: physical activity (shown on normalised scale where 1 represents the maximum value); orange: model prediction with circadian rhythm and integrating activity. (d) the amount of variance of the HRV ($RMSSD^{-1}$) signal explained by circadian rhythms (light orange), a combined model with circadian rhythms and physical activity (medium orange) and a combined model with circadian rhythms, physical activity and HR (dark orange). (e,f) Examples comparing HRV data with model predictions for two participants. Red: HRV data; black: baseline circadian rhythm; green: physical activity (shown on normalised scale where 1 represents the maximum value); orange: model prediction using circadian rhythms, physical activity and HR.

Fig. 5. Adding physical activity, HR and HRV into the glucose dynamics model can help explain glucose dynamics. (a,b,c) Posterior distributions (shown as boxplots) of the model coefficients $C_{5,1}$, $C_{5,2}$, $C_{5,3}$ across all participants, which correspond to the influence on glucose of physical activity, HR and HRV, respectively. The boxplots represent the 25th, median (50th) and 75th percentiles of the posterior distribution and the whiskers represent the 5th and 95th percentiles. (d) A comparison of the variance explained in the glucose signal using just the meal and circadian rhythm model (light orange) compared to the prediction that also incorporates physical activity, HR and HRV (dark orange). (e) Example from ID 06 shows that the physical and heart activity data partially explain an exercise-induced glucose spike. Blue: glucose data; light orange: prediction using meal and circadian model components; dark orange: prediction including meal and circadian model components, physical activity, HR and HRV; brown: the weighted sum of the physical activity, HR and HRV variables according to the inferred coefficients $C_{5,1}$, $C_{5,2}$ and $C_{5,3}$. The timestamps of meals are shown as black dashed lines. (f) Example from ID 08 showing how glucose dynamics (blue) track with the weighted sum of the physical activity, HR and HRV variables according to the inferred coefficients $C_{5,1}$, $C_{5,2}$ and $C_{5,3}$ (dark brown: data only; light brown: using filtered estimations from Model 2 to fill missing Actiheart data). The timestamps of meals are shown as black dashed lines. (g) the cross-

medRxiv preprint doi: https://doi.org/10.1101/2022.08.20.22278813; this version posted August 22, 2022. The copyright holder for this preprint **(which was not certified by peer review)** is the author/funder, who has granted medRxiv a license to display the preprint in perpetuity.
It is made available under a CC-BY-ND 4.0 International license .

correlation of the glucose (blue in (f)) with the weighted sum of the physical activity, HR and HRV variables (brown in (f)) using all recorded data.

References

1. Trachana, K. *et al.* Taking systems medicine to heart. *Circ. Res.* **122**, 1276–1289 (2018).
2. Tirone, T. A. & Brunicardi, F. C. Overview of glucose regulation. *World J. Surg.* **25**, 461–467 (2001).
3. Kahn, S. E., Cooper, M. E. & Del Prato, S. Pathophysiology and treatment of type 2 diabetes: Perspectives on the past, present, and future. *Lancet* **383**, 1068–1083 (2014).
4. Forbes, J. M. & Fotheringham, A. K. Vascular complications in diabetes: old messages, new thoughts. *Diabetologia* **60**, 2129–2138 (2017).
5. Sarwar, N. *et al.* Diabetes mellitus, fasting blood glucose concentration, and risk of vascular disease: A collaborative meta-analysis of 102 prospective studies. *Lancet* **375**, 2215–2222 (2010).
6. Selvin, E. *et al.* Glycated Hemoglobin, Diabetes, and Cardiovascular Risk in Nondiabetic Adults. *N. Engl. J. Med.* **362**, 800–811 (2010).
7. Coutinho, M., Gerstein, H. C., Wang, Y. & Yusuf, S. The relationship between glucose and incident cardiovascular events. *Diabetes Care* **22**, 233–240 (1999).
8. Hansen, E. A. *et al.* Accuracy, satisfaction and usability of a flash glucose monitoring system among children and adolescents with type 1 diabetes attending a summer camp. *Pediatr. Diabetes* **19**, 1276–1284 (2018).
9. Ceriello, A., Monnier, L. & Owens, D. Glycaemic variability in diabetes: clinical and therapeutic implications. *Lancet Diabetes Endocrinol.* **7**, 221–230 (2019).
10. Battelino, T. *et al.* Clinical targets for continuous glucose monitoring data interpretation: Recommendations from the international consensus on time in range. *Diabetes Care* **42**, 1593–1603 (2019).
11. Danne, T. *et al.* International consensus on use of continuous glucose monitoring. *Diabetes Care* **40**, 1631–1640 (2017).
12. Zeevi, D. *et al.* Personalized Nutrition by Prediction of Glycemic Responses. *Cell* **163**, 1079–1095 (2015).
13. Korem, T. *et al.* Bread Affects Clinical Parameters and Induces Gut Microbiome-Associated Personal Glycemic Responses. *Cell Metab.* **25**, 1243-1253.e5 (2017).
14. Berry, S. E. *et al.* Human postprandial responses to food and potential for precision nutrition. *Nat. Med.* **26**, 964–973 (2020).
15. Curtis, A. M. *et al.* Circadian variation of blood pressure and the vascular response to asynchronous stress. *Proc. Natl. Acad. Sci. U. S. A.* **104**, 3450–5 (2007).
16. Levi, F. & Schibler, U. Circadian Rhythms: Mechanisms and Therapeutic Implications. *Annu. Rev. Pharmacol. Toxicol.* **47**, 593–628 (2007).
17. Van Cauter, E., Polonsky, K. S. & Scheen, A. J. Roles of circadian rhythmicity and sleep in human glucose regulation. *Endocr. Rev.* **18**, 716–738 (1997).
18. Stenvers, D. J., Scheer, F. A. J. L., Schrauwen, P., la Fleur, S. E. & Kalsbeek,

medRxiv preprint doi: https://doi.org/10.1101/2022.08.20.22278813; this version posted August 22, 2022. The copyright holder for this preprint **(which was not certified by peer review)** is the author/funder, who has granted medRxiv a license to display the preprint in perpetuity.
It is made available under a CC-BY-ND 4.0 International license .

A. Circadian clocks and insulin resistance. *Nat. Rev. Endocrinol.* **15**, 75–89 (2019).
19. Asher, G. & Sassone-Corsi, P. Time for food: The intimate interplay between nutrition, metabolism, and the circadian clock. *Cell* **161**, 84–92 (2015).
20. Qian, J. & Scheer, F. A. J. L. Circadian System and Glucose Metabolism: Implications for Physiology and Disease. *Trends Endocrinol. Metab.* **27**, 282–293 (2016).
21. Dickmeis, T. Glucocorticoids and the circadian clock. *Journal of Endocrinology* **200**, 3–22 (2009).
22. Ramsey, K. *et al.* Circadian Clock Feedback Cycle Through NAMPT-Mediated NAD + Biosynthesis. *Science (80-.).* **324**, 651–654 (2009).
23. Flanagan, A., Bechtold, D. A., Pot, G. K. & Johnston, J. D. Chrono-nutrition: From molecular and neuronal mechanisms to human epidemiology and timed feeding patterns. *J. Neurochem.* **157**, 53–72 (2021).
24. Aparicio, N. J. *et al.* Circadian variation of the blood glucose, plasma insulin and human growth hormone levels in response to an oral glucose load in normal subjects. *Diabetes* **23**, 132–137 (1974).
25. Porcellati, F., Lucidi, P., Bolli, G. B. & Fanelli, C. G. Thirty Years of Research on the Dawn Phenomenon: Lessons to Optimize Blood Glucose Control in Diabetes. *Diabetes Care* **36**, 3860–3862 (2013).
26. Schmidt, M. I., Hadji-Georgopoulos, A., Rendell, M., Margolis, S. & Kowarski, A. The dawn phenomenon, an early morning glucose rise: Implications for diabetic intraday blood glucose variation. *Diabetes Care* **4**, 579–585 (1981).
27. Johnson, M. L. *et al.* Utilizing the Ambulatory Glucose Profile to Standardize and Implement Continuous Glucose Monitoring in Clinical Practice. *Diabetes Technol. Ther.* **21**, S2-17-S2-25 (2019).
28. Shaffer, F. & Ginsberg, J. P. An Overview of Heart Rate Variability Metrics and Norms. *Front. Public Heal.* **5**, 1–17 (2017).
29. Shaffer, F., McCraty, R. & Zerr, C. L. A healthy heart is not a metronome: an integrative review of the heart's anatomy and heart rate variability. *Front. Psychol.* **5**, 1–19 (2014).
30. Wehrwein, E. A., Orer, H. S. & Barman, S. M. Overview of the Anatomy, Physiology, and Pharmacology of the Autonomic Nervous System. *Compr. Physiol.* **6**, 1239–1278 (2016).
31. Singh, J. P. *et al.* Association of hyperglycemia with reduced heart rate variability (The Framingham Heart Study). *Am. J. Cardiol.* **86**, 309–312 (2000).
32. Wu, J. S. *et al.* Epidemiological evidence of altered cardiac autonomic function in subjects with impaired glucose tolerance but not isolated impaired fasting glucose. *J. Clin. Endocrinol. Metab.* **92**, 3885–3889 (2007).
33. Ewing, D. ., Campbell, I. . & Clarke, B. . Mortality in diabetic autonomic neuropathy. *Lancet* **307**, 601–603 (1976).
34. Gill, S. & Panda, S. A Smartphone App Reveals Erratic Diurnal Eating Patterns in Humans that Can Be Modulated for Health Benefits. *Cell Metab.* **22**, 789–798 (2015).
35. Chow, L. S. *et al.* Time-Restricted Eating Effects on Body Composition and Metabolic Measures in Humans who are Overweight: A Feasibility Study. *Obesity* **28**, 860–869 (2020).
36. Bolie, V. W. Coefficients of normal blood glucose regulation. *J. Appl. Physiol.* **16**, 783–788 (1961).
37. Wyatt, P. *et al.* Energy Intake in Healthy Individuals. *Nat. Metab.* **3**, (2021).

medRxiv preprint doi: https://doi.org/10.1101/2022.08.20.22278813; this version posted August 22, 2022. The copyright holder for this preprint **(which was not certified by peer review)** is the author/funder, who has granted medRxiv a license to display the preprint in perpetuity.
It is made available under a CC-BY-ND 4.0 International license .

38. Schroeder, E. B. *et al.* Diabetes, Glucose, Insulin, and Heart Rate Variability. *Diabetes Care* **28**, 668–674 (2005).
39. Tambascia, M. A. ntoni., Malerbi, D. A. ugust. C. & Eliaschewitz, F. G. oldber. Influence of gastric emptying on the control of postprandial glycemia: physiology and therapeutic implications. *Einstein (Sao Paulo).* **12**, 251–253 (2014).
40. Moore, M. C., Coate, K. C., Winnick, J. J., An, Z. & Cherrington, A. D. Regulation of hepatic glucose uptake and storage in vivo. *Adv. Nutr.* **3**, 286–294 (2012).
41. Bansal, P. & Wang, Q. Insulin as a physiological modulator of glucagon secretion. *Am. J. Physiol. - Endocrinol. Metab.* **295**, (2008).
42. Saad, A. *et al.* Diurnal pattern to insulin secretion and insulin action in healthy individuals. *Diabetes* **61**, 2691–2700 (2012).
43. Chaix, A., Manoogian, E. N. C., Melkani, G. C. & Panda, S. Time-Restricted Eating to Prevent and Manage Chronic Metabolic Diseases. *Annu. Rev. Nutr.* **39**, 291–315 (2019).
44. Cobelli, C. *et al.* Diabetes : Models , Signals , and Control. **2**, 54–96 (2009).
45. Pattaranit, R. & Van Den Berg, H. A. Mathematical models of energy homeostasis. *J. R. Soc. Interface* **5**, 1119–1135 (2008).
46. McGrath, T., Murphy, K. G. & Jones, N. S. Quantitative approaches to energy and glucose homeostasis: Machine learning and modelling for precision understanding and prediction. *J. R. Soc. Interface* **15**, 1–33 (2018).
47. Dalla Man, C., Caumo, A. & Cobelli, C. The oral glucose minimal model: Estimation of insulin sensitivity from a meal test. *IEEE Trans. Biomed. Eng.* **49**, 419–429 (2002).
48. Dalla Man, C., Rizza, R. A. & Cobelli, C. Meal simulation model of the glucose-insulin system. *IEEE Trans. Biomed. Eng.* **54**, 1740–1749 (2007).
49. Soru, P. *et al.* MPC based Artificial Pancreas: Strategies for individualization and meal compensation. *Annu. Rev. Control* **36**, 118–128 (2012).
50. Toffanin, C. *et al.* Artificial pancreas: Model predictive control design from clinical experience. *J. Diabetes Sci. Technol.* **7**, 1470–1483 (2013).
51. Li, K., Daniels, J., Liu, C., Herrero, P. & Georgiou, P. Convolutional Recurrent Neural Networks for Glucose Prediction. *IEEE J. Biomed. Heal. Informatics* **24**, 603–613 (2020).
52. Rubin-Falcone, H., Fox, I. & Wiens, J. Deep residual time-series forecasting: Application to blood glucose prediction. *CEUR Workshop Proc.* **2675**, 105–109 (2020).
53. Miller, A. C., Foti, N. J. & Fox, E. Learning Insulin-Glucose Dynamics in the Wild. 1–25 (2020).
54. Deng, Y. *et al.* Deep transfer learning and data augmentation improve glucose levels prediction in type 2 diabetes patients. *npj Digit. Med.* **4**, (2021).
55. Woldaregay, A. Z. *et al.* Data-driven modeling and prediction of blood glucose dynamics: Machine learning applications in type 1 diabetes. *Artif. Intell. Med.* **98**, 109–134 (2019).
56. Bent, B. *et al.* Engineering digital biomarkers of interstitial glucose from noninvasive smartwatches. *npj Digit. Med.* **4**, 1–11 (2021).
57. Rashtian, H., Torbaghan, S. S., Rahili, S., Snyder, M. & Aghaeepour, N. Heart Rate and CGM Feature Representation Diabetes Detection from Heart Rate: Learning Joint Features of Heart Rate and Continuous Glucose Monitors Yields Better Representations. *IEEE Access* **9**, 83234–83240 (2021).

medRxiv preprint doi: https://doi.org/10.1101/2022.08.20.22278813; this version posted August 22, 2022. The copyright holder for this preprint **(which was not certified by peer review)** is the author/funder, who has granted medRxiv a license to display the preprint in perpetuity.
It is made available under a CC-BY-ND 4.0 International license .

58. Roy, A. & Parker, R. S. Dynamic modeling of exercise effects on plasma glucose and insulin levels. *J. Diabetes Sci. Technol.* **1**, 338–347 (2007).
59. Zhu, T. *et al.* Enhancing self-management in type 1 diabetes with wearables and deep learning. *npj Digit. Med. 2022 51* **5**, 1–11 (2022).
60. Coorey, G., Figtree, G. A., Fletcher, D. F. & Redfern, J. The health digital twin: advancing precision cardiovascular medicine. *Nat. Rev. Cardiol.* **18**, 803–804 (2021).
61. Kamel Boulos, M. N. & Zhang, P. Digital twins: From personalised medicine to precision public health. *J. Pers. Med.* **11**, (2021).
62. Craig, C. L. *et al.* International physical activity questionnaire: 12-Country reliability and validity. *Med. Sci. Sports Exerc.* **35**, 1381–1395 (2003).
63. Roenneberg, T., Wirz-Justice, A. & Merrow, M. Life between clocks: Daily temporal patterns of human chronotypes. *J. Biol. Rhythms* **18**, 80–90 (2003).
64. Buysse, D. J., Reynolds, C. F., Monk, T. H., Berman, S. R. & Kupfer, D. J. The Pittsburgh sleep quality index: A new instrument for psychiatric practice and research. *Psychiatry Res.* **28**, 193–213 (1989).
65. Martín Abadi et al. TensorFlow: Large-Scale Machine Learning on Heterogeneous Distributed Systems. (2015).

medRxiv preprint doi: https://doi.org/10.1101/2022.08.20.22278813; this version posted August 22, 2022. The copyright holder for this preprint (which was not certified by peer review) is the author/funder, who has granted medRxiv a license to display the preprint in perpetuity.
It is made available under a CC-BY-ND 4.0 International license .

Figure 1.

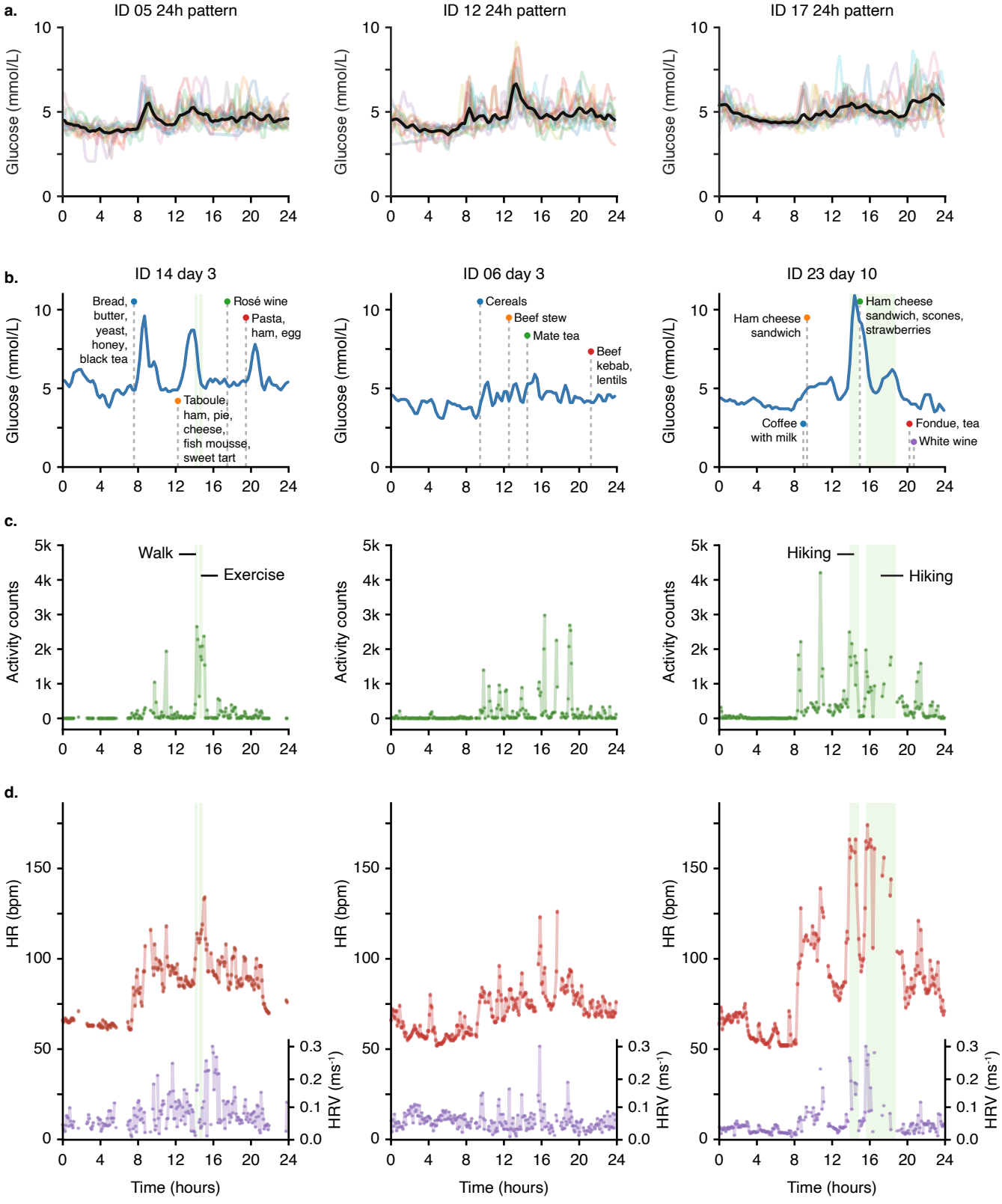

medRxiv preprint doi: https://doi.org/10.1101/2022.08.20.22278813; this version posted August 22, 2022. The copyright holder for this preprint (which was not certified by peer review) is the author/funder, who has granted medRxiv a license to display the preprint in perpetuity.
It is made available under a CC-BY-ND 4.0 International license .

Figure 2.

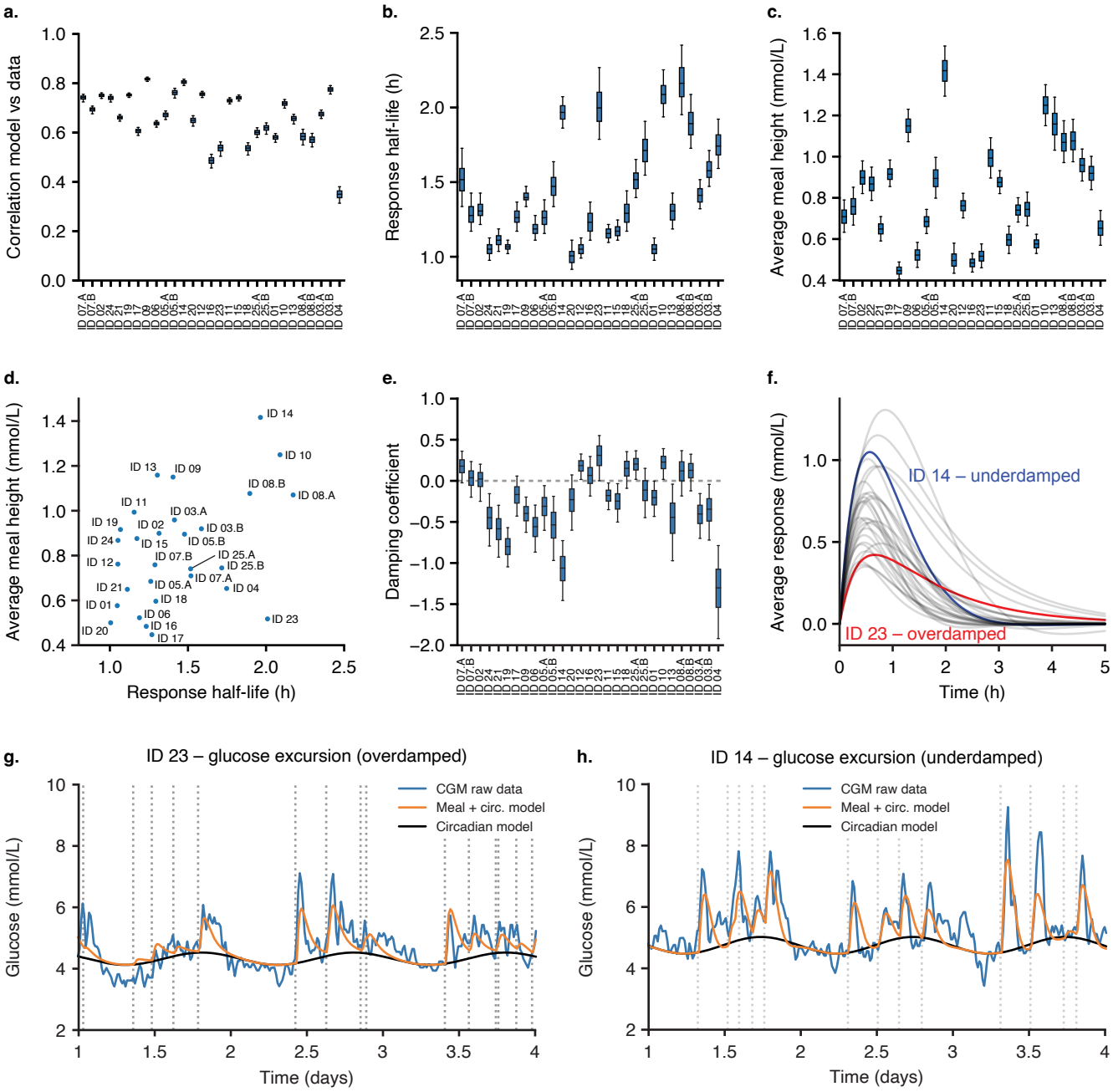

medRxiv preprint doi: https://doi.org/10.1101/2022.08.20.22278813; this version posted August 22, 2022. The copyright holder for this preprint (which was not certified by peer review) is the author/funder, who has granted medRxiv a license to display the preprint in perpetuity.
It is made available under a CC-BY-ND 4.0 International license .

Figure 3.

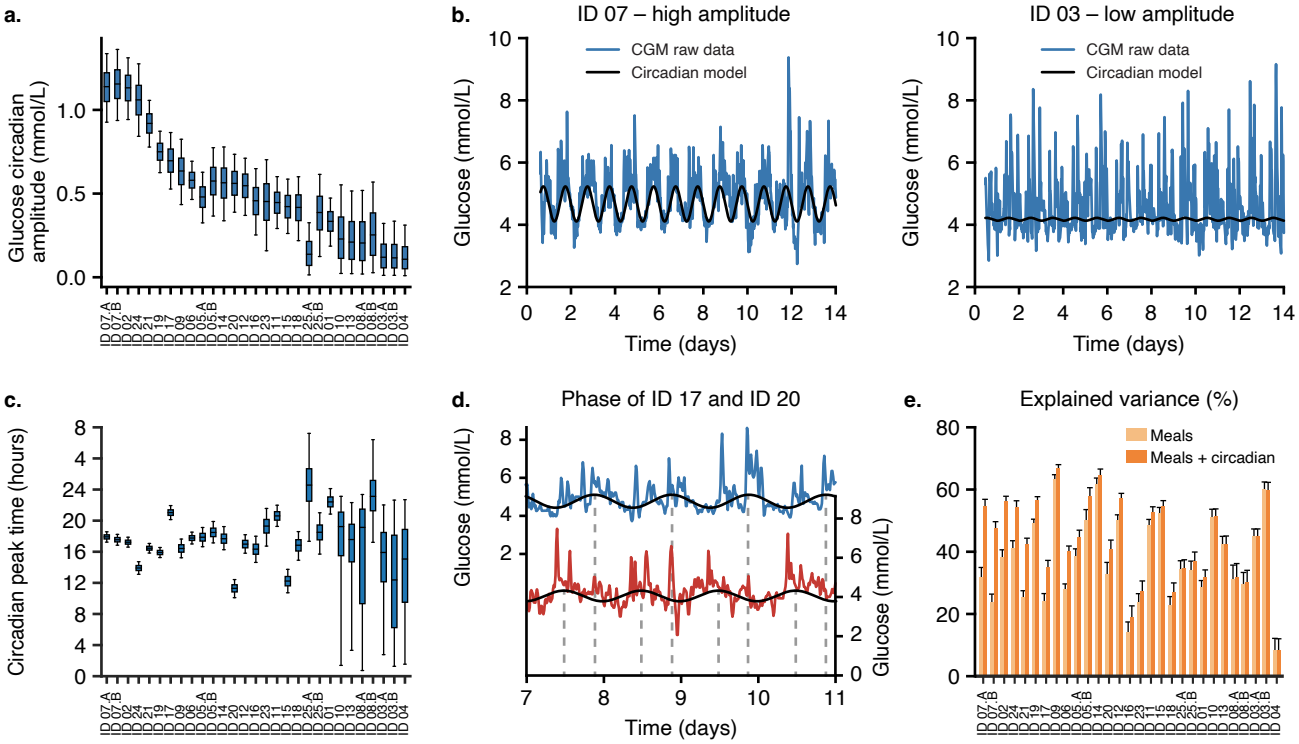

medRxiv preprint doi: https://doi.org/10.1101/2022.08.20.22278813; this version posted August 22, 2022. The copyright holder for this preprint **(which was not certified by peer review)** is the author/funder, who has granted medRxiv a license to display the preprint in perpetuity.
It is made available under a CC-BY-ND 4.0 International license .

Figure 4.

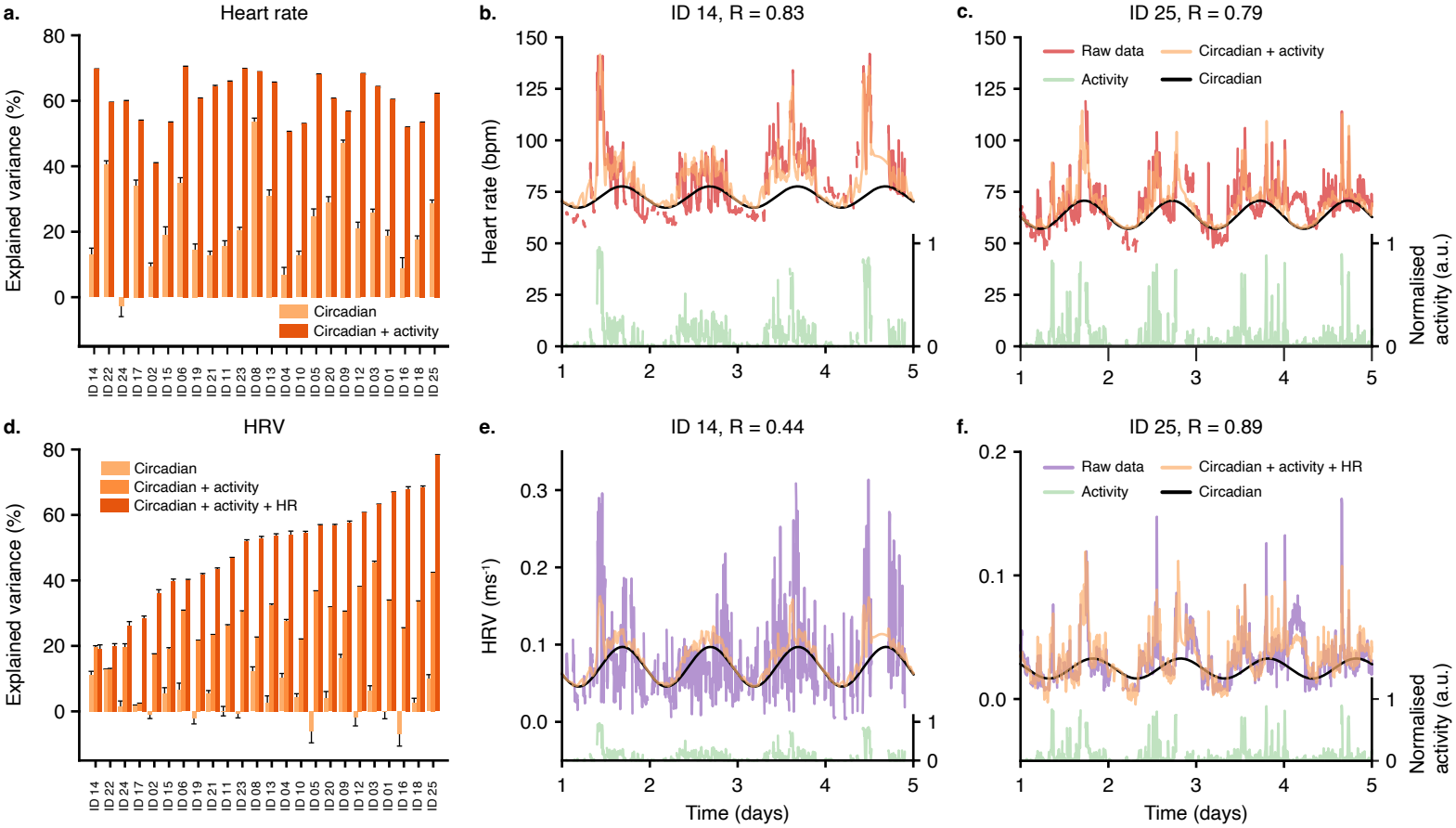

medRxiv preprint doi: https://doi.org/10.1101/2022.08.20.22278813; this version posted August 22, 2022. The copyright holder for this preprint (which was not certified by peer review) is the author/funder, who has granted medRxiv a license to display the preprint in perpetuity.
It is made available under a CC-BY-ND 4.0 International license .

Figure 5.